K_V1/D-type potassium channels inhibit the excitability of bronchopulmonary vagal afferent nerves

Hui Sun [ID], Mayur J. Patil, Fei Ru, Sonya Meeker and Bradley J. Undem [ID]

Division of Allergy and Clinical Immunology, Department of Medicine, Johns Hopkins University School of Medicine, Baltimore, MD, USA

Edited by: Harold Schultz & Andrew Holmes

Linked articles: This article is highlighted in a Perspective article by Yu. To read this article, visit https://doi.org/10.1113/JP283205.

The peer review history is available in the Supporting information section of this article (https://doi.org/10.1113/JP282803#support-information-section).
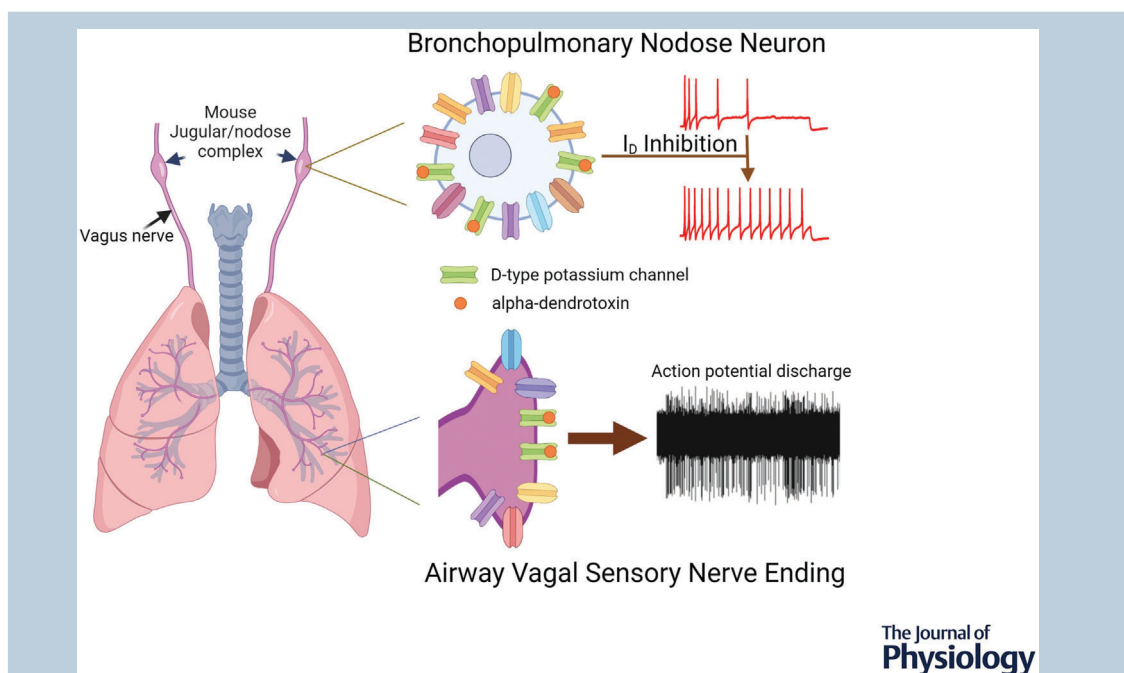
Abstract The K_V1/D-type potassium current (I_D) is an important determinant of neuronal excitability. This study explored whether and how I_D channels regulate the activation of broncho-pulmonary vagal afferent nerves. The single-neuron RT-PCR assay revealed that nearly all mouse bronchopulmonary nodose neurons expressed the transcripts of α-dendrotoxin (α-DTX)-sensitive, I_D channel-forming $K_V1.1$, $K_V1.2$ and/or $K_V1.6$ α-subunits, with the expression of $K_V1.6$ being most prevalent. Patch-clamp recordings showed that I_D, defined as the α-DTX-sensitive K^+ current, activated at voltages slightly more negative than the resting membrane potential in lung-specific

Hui Sun was originally trained in Medicine in China and France. She subsequently obtained her PhD degree on Biomedical Engineering from Claude Bernard University Lyon 1, and received her post-doctoral training on Ion Channel Electrophysiology in Montreal Heart Institute. She is now a faculty member at Johns Hopkins University School of Medicine. Her current research interest is to elucidate the role of potassium channels in the regulation of airway sensory nerve excitability in health and in disease.

nodose neurons and displayed little inactivation at subthreshold voltages. Inhibition of I_D channels by α-DTX depolarized the lung-specific nodose neurons and caused an increase in input resistance, decrease in rheobase, as well as increase in action potential number and firing frequency in response to suprathreshold current steps. Application of α-DTX to the lungs via trachea in the mouse *ex vivo* vagally innervated trachea–lungs preparation led to action potential discharges in nearly half of bronchopulmonary nodose afferent nerve fibres, including nodose C-fibres, as detected by the two-photon microscopic Ca^{2+} imaging technique and extracellular electrophysiological recordings. In conclusion, I_D channels act as a critical brake on the activation of bronchopulmonary vagal afferent nerves by stabilizing the membrane potential, counterbalancing the subthreshold depolarization and promoting the adaptation of action potential firings. Down-regulation of I_D channels, as occurs in various inflammatory diseases, may contribute to the enhanced C-fibre activity in airway diseases that are associated with excessive coughing, dyspnoea, and reflex bronchospasm and secretions.

Corresponding author H. Sun: Division of Allergy and Clinical Immunology, JHAAC 3A.31, 5501 Hopkins Bayview Circle, Baltimore, MD 21224, USA. Email: huisun@jhu.edu

Abstract figure legend Bronchopulmonary vagal sensory nerves express the α-dendrotoxin (α-DTX)-sensitive K_V1-mediated D-type potassium channels that generate a low threshold-activated, fast activating and slowly inactivating K^+ current referred to as I_D. Inhibition of I_D channels in the patch-clamped cell soma of bronchopulmonary nodose afferent neurons with α-DTX enhanced neuronal excitability and increased action potential firing frequency in response to suprathreshold stimuli. Application of α-DTX to the receptive field of vagal sensory nerve endings in the lungs evoked action potential discharge in $\sim$50% of bronchopulmonary C-fibres. Thus, I_D channels can act as a brake on the activation of airway nociceptive afferent nerves. Down-regulation of I_D channels may contribute to the exaggerated nocifensive reflex responses, such as excessive bronchospasm and non-productive coughing, that are often associated with inflammatory airway diseases.

Key points

- The α-dendrotoxin (α-DTX)-sensitive D-type K^+ current (I_D) is an important determinant of neuronal excitability.
- Nearly all bronchopulmonary nodose afferent neurons in the mouse express I_D and the transcripts of α-DTX-sensitive, I_D channel-forming $K_V1.1$, $K_V1.2$ and/or $K_V1.6$ α-subunits.
- Inhibition of I_D channels by α-DTX depolarizes the bronchopulmonary nodose neurons, reduces the minimal depolarizing current needed to evoke an action potential (AP) and increases AP number and AP firing frequency in response to suprathreshold stimulations.
- Application of α-DTX to the lungs *ex vivo* elicits AP discharges in about half of bronchopulmonary nodose C-fibre terminals.
- Our novel finding that I_D channels act as a critical brake on the activation of bronchopulmonary vagal afferent nerves suggests that their down-regulation, as occurs in various inflammatory diseases, may contribute to the enhanced C-fibre activity in airway inflammation associated with excessive respiratory symptoms.

Introduction

The airways, from the larynx to lung parenchyma, are densely innervated by sensory nerves. Their function is to transmit sensory information from the pulmonary tissue to the central nervous system, which is essential for the dynamic regulation of breathing and initiation of adequate airway defensive reflexes. The majority of bronchopulmonary sensory nerve fibres are derived from neurons situated in the vagal sensory ganglia (jugular and nodose ganglia) and travel in the vagus nerve. Aberrant activation of bronchopulmonary vagal sensory nerves in airway inflammatory diseases, such as asthma and chronic obstructive pulmonary disease, are likely contributors to exaggerated dyspnoea, excessive mucous secretion, bronchoconstriction and chronic unproductive cough (Lee & Yu, 2014; Mazzone & Undem, 2016). Understanding the control of bronchopulmonary sensory nerve activation is therefore important for elucidating the pathophysiology of respiratory diseases as well as for

identifying novel therapeutic targets aimed at treating these disorders.

The voltage-gated potassium (K_V) channels constitute the largest ion channel family, comprising 40 α-subunits grouped into 12 subfamilies (K_V1–K_V12) (Gutman et al., 2005). The K_V channels exert powerful control on neuronal excitability. Little is known about the electrophysiological properties and functions of K_V channels with identified molecular basis in the airway sensory nerves. The K_V1 subfamily consists of eight pore-forming α-subunits ($K_V1.1$–$K_V1.8$ encoded by *KCNA* genes *KCNA1–7* and *KCNA10*) that can generate both inactivating and delayed rectifier (non-inactivating) K^+ currents with distinct biophysical and pharmacological properties (Ovsepian et al., 2016). Three K_V1 α-subunits, $K_V1.1$, 1.2 and 1.6, are highly sensitive to α-dendrotoxin (α-DTX) (Harvey, 2001). In native neurons, these three α-DTX-sensitive α-subunits mainly assemble into heterotetrameric K^+ channels (sometimes containing $K_V1.4$ or $K_V1.3$ α-subunit) (Coleman et al., 1999; Koch et al., 1997; Scott et al., 1994; Shamotienko et al., 1997; Wang et al., 1999) that retain their unique pharmacological property and give rise to a low-threshold, fast activating and slowly inactivating K^+ current referred to as the D-type K^+ current (I_D) (Glazebrook et al., 2002; Harvey, 2001; Shen et al., 2004; Storm, 1988). I_D current has been described in various central and peripheral neurons where it plays a role in controlling the generation, timing, pattern or frequency of action potential (AP) firing (Catacuzzeno et al., 2008; Glazebrook et al., 2002; Kline et al., 2005; Shen et al., 2004; Storm, 1988). Deletion of *Kcna1*/$K_V1.1$ or *Kcna2*/$K_V1.2$ in rodents results in epilepsy (Brew et al., 2007; Robbins & Tempel, 2012; Smart et al., 1998). In peripheral sensory system, it has been shown that the I_D channel is an important determinant of the threshold sensitivities of cutaneous mechanoreceptors (Hao et al., 2013) and cold-thermosensitive afferent nerves (Madrid et al., 2009), as well as the hypoxia-induced afferent chemosensory responses (Kline et al., 2005). Genetic inactivation of $K_V1.1$, down-regulation of K_V 1.2, or pharmacological inhibition of I_D caused mechanical allodynia, hypersensitivity to cold and neuropathic pain (Gonzalez et al., 2017; Hao et al., 2013; Zhao et al., 2013). The physiological importance of I_D channels is further highlighted by the facts that mutations in $K_V1.1$ subunit are associated with the human autosomal dominant disease episodic ataxia type 1 with myotonia (Kullmann & Hanna, 2002) and that auto-antibodies against $K_V1.1$, 1.2 and 1.6 are found in patients with acquired neuromyotonia characterized by peripheral nerve hyperexcitability due to a reduction of K_V1 channel expression (Kleopa et al., 2006).

Whether and how I_D channels regulate the activation of bronchopulmonary vagal afferent nerves has remained unexplored. In this study, we characterized the expression profile of D-type K^+ channel-forming α-subunits as well as the biophysical properties and functions of I_D in mouse bronchopulmonary vagal sensory neurons using single-neuron RT-PCR and patch clamp techniques. Moreover, we used the two-photon microscopic Ca^{2+} imaging and extracellular electrophysiological recording techniques to evaluate the role of I_D channels in regulating the activation of vagal afferent nerves terminating in the lungs.

Methods

Ethical approval

All animal experiments in this study were approved by the Institutional Animal Care and Use Committee at the Johns Hopkins University School of Medicine (reference no. MO19M151). We as investigators understand the ethical principles under which *The Journal* operates and our work complies with the animal ethics checklist as described in the editorial by Grundy (2015).

Animals

Eight- to 12-week-old male mice (C57BL/6J) were used for experiments. The wild-type mice were purchased from The Jackson Laboratory (Bar Harbor, ME, USA). Transgenic mice with Ca^{2+} sensitive protein GCaMP6s exclusively expressed in the sensory neurons (*Pirt-Cre;R26-GCaMP6s*) were generated by crossing the pan-sensory neuron promoter Pirt-driven Cre (Pirt-Cre) expressing mice (originally generated by X. Dong's laboratory at the Johns Hopkins University) with the ROSA26-lsl-GCaMP6s mouse line. The latter was originally provided by D. Bergles at the Johns Hopkins University and is now commercially available from The Jackson Laboratory. The animals were housed in an approved animal facility under a 12:12 h light–dark cycle with controlled temperature and humidity, and allowed to access food and water *ad libitum*.

Retrograde labelling

The bronchopulmonary afferent neurons in the vagal ganglia (or jugular–nodose complex in the case of mouse) were retrogradely labelled with 1,1′-dioctadecyl-3,3,3′,3′-tetramethylindocarbocyanine perchlorate (DiI; Thermo Fisher Scientific, Waltham, MA, USA) or WGA488 (wheat germ agglutinin, Alexa Fluor 488 conjugate, Thermo Fisher Scientific). One per cent of DiI stock solution was prepared with dimethyl sulfoxide (DMSO). On the day of labelling, this stock solution was diluted 10 times with saline. WGA488 (5 mg) was dissolved in a mixture of 5 μl DMSO and 500 μl filtered

Dulbecco's Phosphate Buffered Saline by vortexing to make up a 1% solution. The DiI stock solution and WGA488 solution were stored at −20°C in a light-proof container.

Mice were anaesthetized with ketamine (80 mg kg^{-1}) and xylazine (10 mg kg^{-1}) intraperitoneally (I.P.). Lack of withdrawal of the hindlimb in response to a pinch between the toes was indicative of adequate anaesthesia. A small midline incision was made in the neck of mouse to expose the trachea. Visualizing the trachea helped ensure that the intubation was precisely intratracheal. The mouse was then orotracheally intubated, and 25 μl of 0.1% DiI or 10−15 μl of 1% WGA488 was instilled into the tracheal lumen just above the bifurcation into the main bronchi. To minimize pain and distress, mice were given 0.05 mg kg^{-1} buprenorphine (S.C.), beginning with anaesthesia and 6 h post-surgery. The animals recovered under close observation for 4−6 h after surgery and were monitored for distress and pain daily. The mice were used for dissociation of nodose neurons 7−10 days post-retrograde labelling.

Dissociation of nodose neurons

Mice were euthanized by CO_2 inhalation and subsequent exsanguinations. Both sides of nodose ganglia were dissected and cleared of adhering connective tissues in ice-cold calcium- and magnesium-free phosphate-buffered saline (PBS; pH 7.4). Since the jugular and nodose neurons are distinct in embryonic origin and phenotype (Nassenstein et al., 2010), this study will focus on nodose neurons. Accordingly, the lower two-thirds of nodose ganglion (with no or minimal jugular component; Nassenstein et al., 2010) was cut out for subsequent enzymatic digestion using type 1A collagenase (2 mg ml^{-1}) and dispase II (2 mg ml^{-1}), as previously described (Sun, 2021). Briefly, the enzymatic digestion proceeded at 37°C for 60 min with gentle trituration of the ganglion tissue at the end of 30, 45 and 60 min of digestion. The dissociated neurons were then washed two times with pre-warmed Leibovitz's L-15 medium supplemented with 10% fetal bovine serum (FBS), plated onto poly-D-lysine/laminin-coated cover glasses and maintained at 37°C in L-15 medium containing 10% FBS for use within 6 h for cell collection (for single-neuron RT-PCR) or within 24 h for patch clamp recordings.

Single-neuron RT-PCR assay

Dissociated unlabelled or retrogradely DiI-labelled nodose neurons were constantly perfused with PBS at room temperature. Labelled neurons were identified under a fluorescence microscope. Single randomly selected or labelled nodose neuron was sucked into a glass pipette with a tip diameter at 50−150 μm. The pipette tip was then broken into a PCR tube (one cell per tube) containing 1 μl RNAse inhibitor (RNaseOUT, Thermo Fisher Scientific; 2 U μl^{-1}) and immediately snap-frozen. A sample of the bath solution from the vicinity of a neuron was collected from each coverslip for no-template experiments (bath control). The neurons were collected between 2 and 6 h post-dissociation.

First-strand cDNA was synthesized using the Super-Script III First-Strand Synthesis System for RT-PCR (cat. no. 18080, Thermo Fisher Scientific) according to the manufacturer's recommendations; 1.5 μl of synthesized cDNA (or RNA control and bath control) was used for PCR amplification (50 cycles) for mouse *P2rx2*, *Trpv1* and *Kcna1−6* using custom-synthesized primers (Sigma-Aldrich, St Louis, MO, USA) (Table 1) and the HotStar Taq Polymerase Kit (Qiagen, Germantown, MD, USA) in a final volume of 20 μl. The PCR protocol consisted of an initial activation step at 95°C for 15 min, and 50 cycles of denaturation at 94°C for 30 s, annealing at 60°C and extension at 72°C for 1 min, followed by a final extension at 72°C for 10 min. PCR products were visualized in ethidium bromide-stained 1.5% agarose gels.

Patch-clamp recording and data analysis

Conventional and amphotericin B-perforated whole cell patch-clamp techniques were employed to record the I_D current and membrane potentials under the voltage-clamp mode and current-clamp mode, respectively, using an Axopatch 200B amplifier interfaced with Axon Digidata 1550A and driven by pCLAMP 10 software (Molecular Devices, San Jose, CA, USA). For I_D recording, the bath solution contained (mM): 136 *N*-methyl-D-glucamine (NMDG)-Cl, 5.4 KCl, 1.5 $MgCl_2$, 0.05 $CaCl_2$, 10 Hepes, and 10 glucose, with pH adjusted to 7.35 with HCl. The pipette solution contained (mM): 125 KCl, 10 NaCl, 0.1 $CaCl_2$, 10 Hepes, 2 EGTA and 5 MgATP, with pH adjusted to 7.2 with KOH. The junction potential (−10 mV, estimated using the Clampex calculator) was corrected during acquisition. Voltage ramp and step commands were used to evaluate I_D. The detailed voltage clamp protocols are given in Results where appropriate. Membrane currents were sampled at 10 kHz and filtered at 2 kHz. The cell capacitance and series resistance (80%) were compensated. For current-clamp experiments, the bath solution contained (mM): 135 NaCl, 5.4 KCl, 1 $MgCl_2$, 1.2 $CaCl_2$, 0.33 NaH_2PO_4, 10 Hepes, and 10 glucose, with pH adjusted to 7.35 with NaOH. Pipette solution contained (mM): 30 KCl, 115 potassium gluconate, and 10 Hepes, with pH adjusted to 7.2 with KOH. Freshly prepared amphotericin B was added to the pipette solution (300 μg ml^{-1}) before experiments. The

Table 1. Single cell RT-PCR primer sequences

Gene	Primer	Sequence	Product length
Kcna1	Forward (5′−3′)	AGTATCCCCGATGCTTTC	250 bp
	Reverse (3′−5′)	GGTCACTGTCAGAGGCTAAG	
Kcna2	Forward (5′−3′)	CATCTGCAAGGGCAACGTCA	432 bp
	Reverse (3′−5′)	GATAACGGCCCCAGGAAACA	
Kcna3	Forward (5′−3′)	AGCTTCTGGTGCGGTTCTTT	132 bp
	Reverse (3′−5′)	TACCTTGTCGTTCAGCCAGC	
Kcna4	Forward (5′−3′)	AACGAGGACTCTGCAATACCC	321 bp
	Reverse (3′−5′)	TTCCAGCAGAGGCAAACTCAA	
Kcna5	Forward (5′−3′)	GTCCGGGTGTTCCGAATCTT	181
	Reverse (3′−5′)	AGAAGTGCGACCCCTGATTG	
Kcna6	Forward (5′−3′)	CTGCTCAAGAAGGTGGGGTT	246 bp
	Reverse (3′−5′)	GGGGTCTCATCCTCCAGAGA	
P2rx2	Forward (5′−3′)	GGG GCA GTG TAG TCA GCA TC	241 bp
	Reverse (3′−5′)	TCA GAA GTC CCA TCC TCC A	
Trpv1	Forward (5′−3′)	TCA CCG TCA GCT CTG TTG TC	285 bp
	Reverse (3′−5′)	GGG TCT TTG AAC TCG CTG TC	

junction potential (-13.8, estimated using the Clampex calculator) was corrected offline.

Patch clamp recordings were analysed using Clampfit 10 (Molecular Devices) and SigmaPlot (Systat Software, Inc., San Jose, CA, USA) software. The steady-state activation of I_D was assessed by measuring tail currents (I_{tail}) at -100 mV following 600-ms voltage steps to different potentials. The amplitude of I_{tail} was measured as the difference between the inward peak and sustained current level at the end of 300 ms hyperpolarization. To obtain the activation parameters, data points were fitted to the Boltzmann function for each neuron: $I_{tail}/I_{tail.max} = G_{max}/(1 + \exp(-(V_m - V_{0.5})/k))$, where G_{max} is maximal conductance, V_m membrane potential, $V_{0.5}$ the voltage at which 50% of activation occurs, and k the slope factor. The input resistance was calculated by dividing the voltage step (5 mV depolarizing step from the resting potential) by sustained current measured at the end of voltage pulse. The rheobase was measured as the lowest amount of depolarizing current (25 ms) needed to evoke a single AP. The AP threshold was measured by differentiating the AP voltage with respect to time (dV/dt) and defined as the voltage at which the deflection for dV/dt is greater than zero.

ventricle. Krebs buffer contained (mM): 118 NaCl, 5.7 KCl, 1 NaH$_2$PO$_4$, 1.2 MgSO$_4$, 1.9 CaCl$_2$, 25 NaHCO$_3$, and 11.1 dextrose, saturated with 95% O$_2$−5% CO$_2$ (pH 7.4). The trachea and lungs, along with the left- and right-side vagus nerves and jugular–nodose ganglia complex (JNC), were dissected. The airway tissue was pinned down in the larger chamber of a Sylgard-lined Perspex tissue bath. The right or left JNC, along with the rostral-most vagus was pulled through a small hole into an adjacent chamber for recording of vagal neuron activities by two-photon microscopic Ca^{2+} imaging or extracellular electrophysiological recording (Fig. 1). The hole was then sealed with Vaseline to prevent the exchange of fluids between the two chambers, which were separately superfused with Krebs solution (35−37°C, 4 ml min^{-1}). A piece of PE60 tubing was inserted into the trachea and connected to the infusion pump for continuous perfusion of the lungs with Krebs solution (35−37°C, 2 ml min^{-1}) and for application of agonists and test compounds. Short cuts (<1 mm deep, 6−10 per lobe) were made on the lung surface to allow perfusate to exit the tissue. The perfusion pressure was recorded by a pressure transducer attached to the model TA240S chart recorder (Gould, Valley View, OH, USA).

Mouse *ex vivo* vagus-innervated trachea–lung preparation

Mice were injected with heparin (200 i.u.) 10 min before euthanization by CO$_2$ inhalation and exsanguination. The blood in the pulmonary circulation was washed out by *in situ* perfusion with Krebs–bicarbonate buffer via the right

Two-photon imaging and data analysis

The two-chamber tissue bath holding the vagally innervated trachea–lung preparation isolated from the *Pirt-Cre;R26GCaMP6s* transgenic mice was mounted firmly on a microscope stage. The tissues in the two chambers were separately and continuously perfused

with Krebs solution saturated with 95% O_2−5% CO_2 (37°C, pH7.4) at 4 ml min^{-1}. A ×20 objective (Scientifica, Clarksburg, NJ, USA) was positioned directly above the nodose ganglion (central-caudal part of JNC) and the piezo drive for the objective was engaged. The ganglial coordinates for the z-stack, starting from top to bottom (100 μm) were adjusted using Labview software (National Instruments, Austin, TX, USA). The live images of the nodose ganglia were acquired at 10 frames per 6 s for a depth of ∼100 μm (i.e. 10 planes of 10 μm-thick slice) with 600 Hz frame scan mode. Before each experiment, the baseline activity of the neurons was recorded and the laser power and the emission gain of the photo-multiplier tube (PMT) were adjusted to have adequately low noise levels. The laser power at 35% and the PMT gain around 750 V were used with our system. The buffer (as Vehicle) and tested compounds (100 nM α-DTX, 10 μM α,β-methylene-ATP (α,β-mATP) and 1 μM capsaicin) were then administrated sequentially via a tracheal cannula to the lungs (3 ml volume each for 1 min application) with an interval of 5−8 min during which the trachea–lungs were continuously washed with Krebs. The recordings were started 30 s before vehicle or test compound application and continued for an additional 5 min to record the neuronal response to vehicle or chemicals. Since the two-photon microscopy uses a laser excitation wavelength of 920 nm, the GCaMP6s experienced no photobleaching and hence there was no loss of fluorescence signals over repetitive stimulation by various compounds.

The acquired live images of nodose ganglia were analysed offline using ImageJ (Fiji). First, the time lapse images of the z-stacks recorded from the same nodose ganglion in response to vehicle and different test compounds were inspected using group z-stack compression. This process examines whether there was any x, y, or z-axis movement of the ganglion during image acquisition. Any movement of the ganglia during recording was corrected using an ImageJ plugin, Stackreg. Next, the z-stack images obtained from the same ganglion at baseline and following the applications of vehicle and various test compounds were concatenated together in the sequence they were acquired. The concatenated images were then divided into 10 substacks (each z-stack divided by 10) which correspond to the 10 frames of images from top to bottom with an increment of 10 μm sampled every 6 s during acquisition. Since mouse sensory neurons are approximately 20 μm in diameter, every other substack (total five out of 10 substacks) was analysed to ensure the same neurons were not counted twice. The neurons were identified on the so selected substack images by marking the regions of interest (ROIs). The fluorescence intensity of the ROIs was measured and analysed further in Excel. The number of responsive neurons was counted as those that had fluorescence intensity >1.5-fold over the base-line in response to vehicle or test compounds. Neurons that responded to buffer alone (vehicle) applied in the same way as test compounds are considered sensitive to distension. These neurons were excluded from the analyses for drug responses unless their responses to the test compounds were >1.5-fold of their response to the vehicle. This group of neurons represents ∼20% of the total neurons analysed in this study (90 out of a total of 455 neurons). The amplitude of increase in the fluorescence signal induced by vehicle or test compounds is expressed as $\Delta F/F_0$, where F_0 denotes the baseline fluorescence
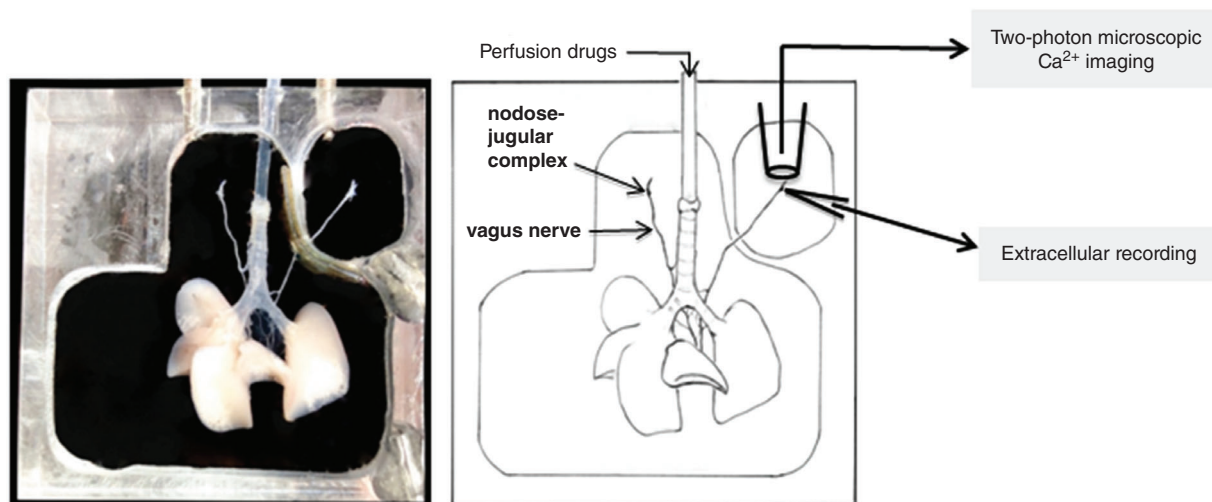
Figure 1. Mouse *ex vivo* vagus-innervated trachea–lung preparation
Photograph and schematic representation showing the mouse trachea–lung preparation along with the intact vagus and vagal ganglia housed in the two-chamber tissue bath for studying bronchopulmonary vagal afferent nerve activities by two-photon microscopic Ca^{2+} imaging or extracellular recording technique. [Colour figure can be viewed at wileyonlinelibrary.com]

intensity and ΔF the changes in the fluorescence intensity from the baseline.

Extracellular recording

The extracellular recordings of action potentials generated from nodose bronchopulmonary C-fibres were carried out *ex vivo* using the vagus-innervated trachea–lung preparation (Fig. 1). After at least 60 min of equilibration, the recording microelectrode with a tip resistance ∼2 MΩ when filled with 3 M sodium chloride was positioned in the lower two-thirds of the JNC (most likely recording nodose neuron) and micromanipulated until a receptive field in the lungs was found. The receptive field of a single C-fibre was searched for and identified with a small concentric electrode (100 V, 0.5 ms, 1 Hz) sequentially positioned at different places on the surface of the lung lobes while the neuronal activity in the JNC was monitored. When electrical stimulation of the tissue evoked action potentials, the tissue was probed with a mechanical probe (von Frey hair, 60−1800 mN). The mechanosensitive receptive field was identified when the mechanical stimulus evoked a burst of action potentials. The recorded electrical signals were amplified (Microelectrode AC Amplifier 1800; A-M Systems, Everett, WA, USA), filtered (0.3 kHz low cutoff and 1 kHz high cutoff), and monitored on an oscilloscope (TDS340; Tektronix, Beaverton, OR, USA) and a chart recorder (TA240; Gould). The scaled output from the amplifier was also captured and analysed by a Macintosh computer using NerveOfIt software (Phocis, Baltimore, MD, USA).

In this study we focused on the nodose bronchopulmonary C-fibres. The conduction velocity was calculated by dividing the distance along the nerve pathway by the time between the shock artifact and the action potential evoked by electrical stimulation of the mechanosensitive receptive field. C-fibres were identified as having a conduction velocity ≤0.7 m s^{-1} (Kollarik & Undem, 2004). Our previous studies also showed that the P2X3-selective agonist α,β-mATP consistently activates nodose C-fibres but not jugular C-fibres (Nassenstein et al., 2010). We therefore first tested the responsiveness of the identified C-fibres to 10 μM α,β-mATP applied to the lungs via trachea as a bolus (1 ml volume in ∼20 s). At least 15 min after α,β-mATP stimulation, the effects of α-DTX (300 nM, 1 ml volume) applied in the same way were evaluated in the α,β-mATP-sensitive C-fibres. The action potential discharge was quantified offline as peak frequency (peak number of action potentials in any 1 s bin) and total number of action potentials (the number of action potentials assessed until the discharge returned to baseline levels, generally <90 s). On the occasion when background activity unrelated to the nerve ending under study was present, NerveOfIt was used to define only those peak shapes that were in precise accordance with the action potential evoked by punctate stimulation of the receptive field. In this way, 'fit spikes' were culled from any background activity.

Statistical analysis

All statistical analyses were performed using SigmaPlot software. Pooled data are expressed as means ± SD. The statistical significance of differences between two means was determined by using either paired or unpaired Student's *t*-test, as appropriate. In the cases that the normality test failed, the Wilcoxon signed-rank test was used. The significance of differences between multiple means or repetitive measurements was evaluated by one-way repeated-measures ANOVA. The Holm–Šidák test as a *post hoc* analysis was performed for multiple pairwise comparisons.

Results

Expression profile of *Kcna*/K$_V$1 α-subunits in mouse nodose and lung-specific nodose neurons

The *Kcna* gene family contains eight members: *Kcna1–7* and *Kcna10*. *Kcna 1*, *2* and *6* encode the α-DTX-sensitive K$_V$1.1, K$_V$1.2 and K$_V$1.6 α-subunits. The *Kcna4*-encoded K$_V$1.4 and *Kcna3*-encoded K$_V$1.3 α-subunits have also been found in some DTX-sensitive heterotetrameric channel complexes purified from brain tissues (Coleman et al., 1999; Koch et al., 1997; Scott et al., 1994; Shamotienko et al., 1997; Wang et al., 1999). Here we examined the expression profile of *Kcna1–6* using the single-neuron RT-PCR assay in randomly picked nodose neurons as well as in neurons specifically innervating the lungs. *P2rx2* expression was used as the marker for nodose neurons (*vs.* jugular neurons) (Nassenstein et al., 2010). We also evaluated *Trpv1* expression as a marker for capsaicin-sensitive C-fibre neurons. As shown in Fig. 2, the expression profile of *Kcna1–6* in nodose neurons innervating the lungs was representative of nodose neurons in general. Also, there was no major distinction in the *Kcna* mRNA expression between the *Trpv1*-positive and *Trpv1*-negative neurons. *Kcna6* transcript was found in almost every neuron examined whereas *Kcna5* transcript was rarely expressed. A large number of neurons also expressed *Kcna1*, *2*, *3* and *4*. The percentage of lung-specific nodose neurons (including both *Trpv1*-positive and -negative ones) expressing *Kcna 1*, *2*,*3* and *4* was 73%, 57%, 37% and 67%, respectively. The absence of all three α-DTX-sensitive subunit transcripts was only noted in 3 out of 30 lung-specific neurons (from four mice), and in 1 out of 30 randomly picked nodose neurons (from four mice), predicting that the majority of

mouse nodose neurons should express α-DTX-sensitive K$^+$ currents.

Characteristics of I_D in mouse lung-specific nodose neurons

I_D current was recorded as the α-DTX- sensitive K$^+$ currents under the conditions where the Na$^+$ currents, Ca^{2+} currents and various non-selective cation currents were eliminated or minimized by replacing the extracellular Na$^+$ with NMDG$^+$ and by using an extremely low concentration of Ca^{2+} (50 μM) in the recording bath solution in this study. Figure 3A gives an example illustrating how I_D was isolated in a lung-specific nodose neuron in response to the voltage ramp from -100 mV to $+20$ mV following a 300 ms hyperpolarizing

step from the holding potential -70 mV to -100 mV. Bath application of 50 nMα-DTX reduced the outward K$^+$ current to different degrees at voltages $\geq \sim -70$ mV in this neuron. The α-DTX-sensitive current, I_D, obtained by digital subtraction of the current recorded in the presence of α-DTX from that recorded before the blocker application exhibits two outward components. The current activates around -70 mV, reaches the first peak around -35 mV, and following a short plateau increases more eminently at stronger depolarization. The α-DTX-sensitive current was observed in nearly all lung-labelled nodose neurons studied (14 of 15 neurons from five mice). The I_D in 12 of these 14 neurons exhibited two outward components with the current starting to activate at -65.7 ± 4.3 mV. In the remaining two neurons the I_D activated at more positive potentials (-40 and -42 mV, respectively) and increased with
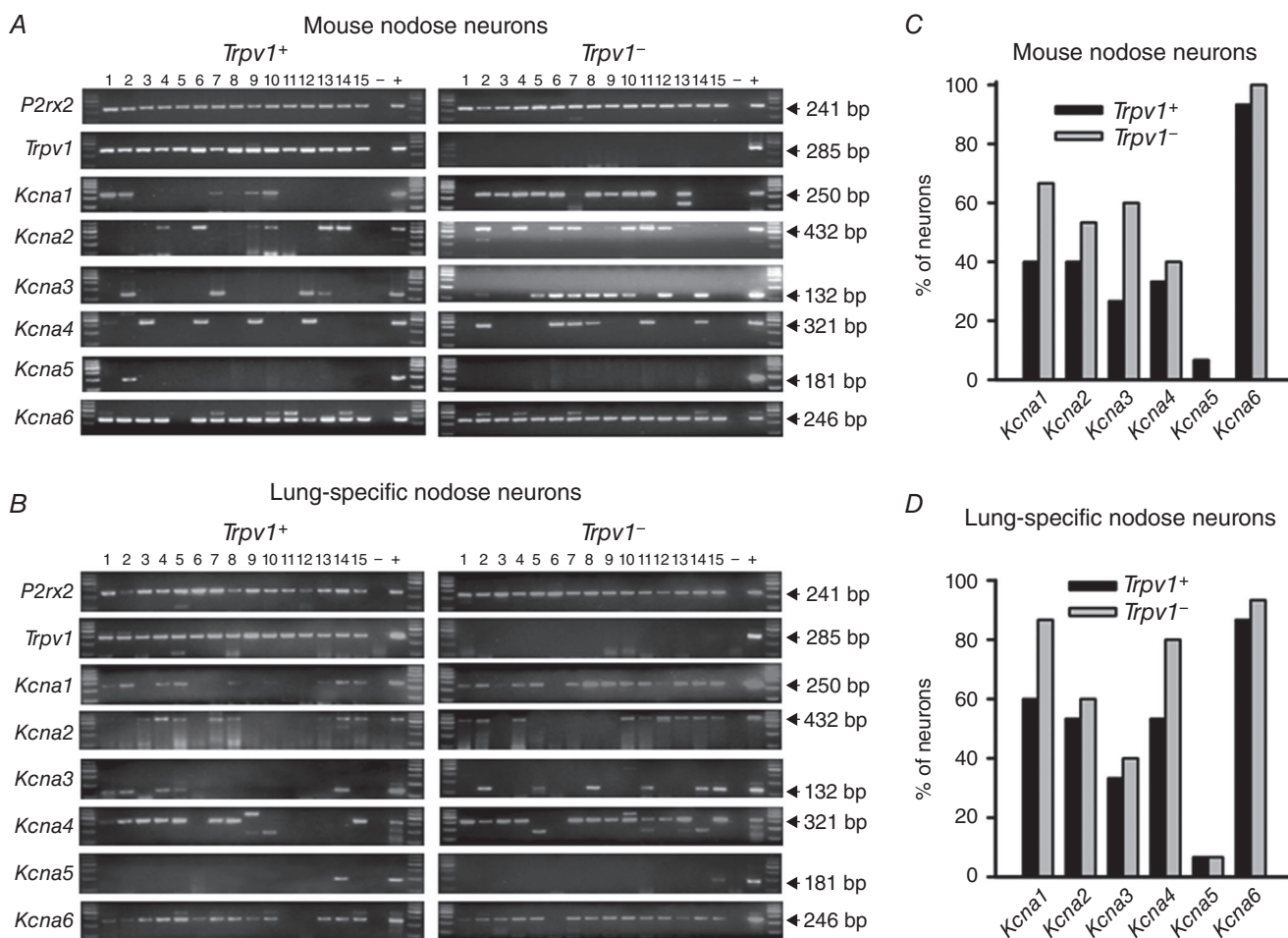

Figure 2. Expression profile of *Kcna1–6* in mouse lung-specific and randomly picked nodose neurons
A and B, gel images showing the amplicons of single-neuron RT-PCR obtained with primers designed to detect *Kcna 1–6* from 15 *Trpv1*-positive and 15 *Trpv1*-negative unlabelled nodose neurons (from four mice), and from 15 *Trpv1*-positive and 15 *Trpv1*-negative lung-specific nodose neurons (from four mice), respectively. *P2rx2* served as the marker for nodose (*vs.* jugular) neurons. Each lane (numbered at the top of the gel images) gives the results obtained from the same one neuron. −, negative control; +, positive control. C and D, bar graphs showing the prevalence of *Kcna 1–6* expression in randomly picked and lung-specific nodose neurons, respectively.

depolarization, similar to the second outward component elicited by stronger depolarization as shown in Fig. 3. Most lung-specific neurons that showed two outward components of I_D in response to voltage ramps had smaller low-threshold components than the one shown in Fig. 3*A*. One example is given in Fig. 3*B*. In a total of 12 neurons, the low-threshold component peaked at -40 ± 5 mV with an amplitude of 7.6 ± 9.0 pA/pF, and the total I_D at $+20$ mV was 52.1 ± 29.2 pA/pF. Although the amplitude of the high-threshold component was markedly greater than the low-threshold component, the latter accounted for a larger percentage of total K$_V$ current at the subthreshold voltages. In the 12 lung-specific nodose neurons displaying two outward components, I_D represented $69.1 \pm 22.2\%$, $58.8 \pm 17.5\%$, $49.8 \pm 16.3\%$ and $36 \pm 17\%$ of the total K$_V$ current recorded at -55, -50, -45 and -40 mV, respectively, while it only accounted for $22.3 \pm 14.2\%$ of the total K$_V$ current at $+20$ mV.

Similarly, two outward components of 50 nм α-DTX-sensitive currents in response to depolarization ramps were observed in randomly picked nodose neurons (14.4 ± 20.3 and 66.3 ± 43.4 pA/pF for the amplitude of low-threshold component and current at $+20$ mV, respectively; $n = 13$ neurons from 8 mice). To verify that the current inhibited by 50 nм α-DTX truly reflects the characteristics of I_D in mouse nodose neurons, we tested the effects of a lower concentration of α-DTX (10 nм) and

a low concentration of 4-aminopyridine (4-AP; 30 μм) on the membrane current in randomly picked nodose neurons under the same experimental conditions. I_D is known to be highly sensitive to low concentrations of 4-AP (Stansfeld et al., 1986; Storm, 1988). The 10 nм α-DTX-sensitive current and 30 μм 4-AP-sensitive current exhibit the similar characteristic of two outward components, as shown in Fig. 3*C*, in 6/7 and 7/10 neurons (from four and three mice), respectively. In the remaining four neurons only the high-threshold component that activated at -34.3 ± 8.3 mV was observed. These findings validate the use of 50 nм α-DTX to isolate the I_D in mouse nodose neurons. The results obtained with the voltage ramp protocol indicate that in the vast majority of mouse lung-specific nodose neurons ($\sim$80%), I_D activates around the resting potentials and accounts for a large proportion of K$^+$ currents available in the subthreshold voltage range albeit its amplitude varies widely among different neurons.

To evaluate the voltage-dependent activation of I_D from a more physiological membrane potential and to examine the activation, deactivation and inactivation kinetics of the current, the α-DTX-sensitive K$^+$ current in response to step voltage commands was recorded in lung-specific nodose neurons. The voltage-clamp protocol (Fig. 4*A*, bottom) was composed of 600-ms steps from a holding potential of -70 mV to voltages between -75 and $+25$ mV with an increment of 10 mV, followed
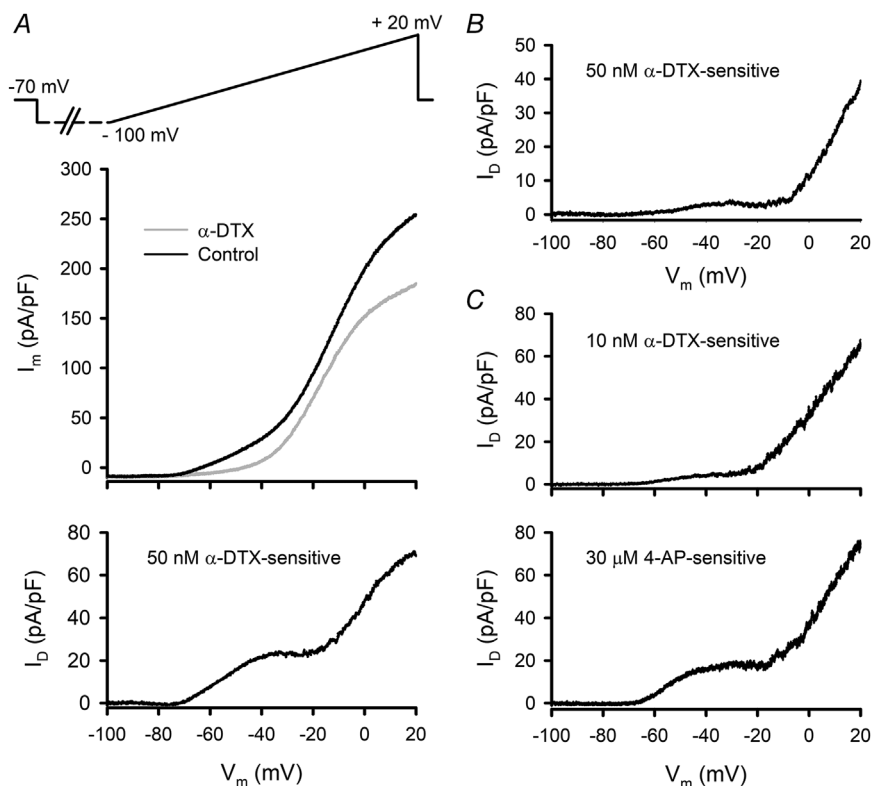

Figure 3. I_D currents elicited by voltage ramps in lung-specific and randomly selected nodose neurons
A, outward K$^+$ currents elicited by the voltage ramp protocol (top) from a lung-specific nodose neuron before and after application of 50 nмα-DTX (middle). I_D, defined as the α-DTX-sensitive current (bottom), was obtained by digital subtraction of the current recorded in the presence of α-DTX from that in the control. *B*, I_D, the 50 nм α-DTX-sensitive current, obtained from another lung-specific nodose neuron. *C*, I_D, defined as the 10 nм α-DTX- or 30 μм 4-AP-sensitive current, obtained from two different randomly picked nodose neurons.

by a 300-ms hyperpolarizing step to -100 mV before stepping back to the holding potential to elicit the tail currents that reflect the steady-state activation of I_D at the end of 600 ms of depolarization. Figure 4*A* shows the representative current recordings obtained from a lung-specific neuron before and during bath application of 50 nMα-DTX. The α-DTX-sensitive current obtained by the digital subtraction reveals that I_D activates rapidly and does not inactivate during 600 ms in this neuron. In four of six neurons (from three mice) studied with the same protocol, I_D exhibited slow inactivation at depolarizing voltages ≥-5 mV. One example is given in Fig. 4*B*. The current–voltage (*I*–*V*) curves for the peak and sustained I_D, I_{peak} and I_{Sus} measured at the current maximum and at the end of 600-ms pulses, respectively, are plotted in Fig. 4*C*. The amplitudes of I_{peak} and I_{sus} are closely similar at voltages ≤-15 mV, suggesting little inactivation of I_D at subthreshold and around threshold voltages. At $+25$ mV, the most positive potential tested in these neurons, $>75\%$ of I_D channels remained open after prolonged depolarization. In a total of 10 lung-specific nodose neurons (from five mice) where I_D was recorded at $+15$ mV for 600 ms, the current displayed little inactivation in five neurons. In the other five neurons, a slow inactivation was observed with the inactivation time constant varying from 173 to

1295 ms (mean 563 ± 442 ms). The activation of I_D also fits the single exponential function. The activation time constant ($\tau_{activation}$) decreased as the depolarization increased (Fig. 4*D*). The averaged $\tau_{activation}$ was <10 ms at voltages ≥-15 mV ($n = 6$ neurons from three mice). At more negative potentials, the $\tau_{activation}$ varied considerably among different neurons (1.1–55 ms at -35 mV, and 1.4–35 ms at -25 mV). The deactivation kinetics of I_D was evaluated by fitting to a single exponential function the decay phase of α-DTX-sensitive I_{tail} elicited by hyperpolarization from voltage steps between -15 and $+25$ mV to -100 mV. The deactivation time constants were found to be 12–14 ms in five neurons from three mice (Fig. 4*D*). The steady-state activation curve of I_D channels was generated by plotting the amplitude of α-DTX-sensitive I_{tail} normalized to the maximal I_{tail} against the voltages preceding the hyperpolarization step (prepulse, Fig. 4*E*). On average, 10–30% of channels were activated at the resting and subthreshold potentials (-65 to -35 mV); an additional 70% of channels activate at suprathreshold potentials; and the activation almost reaches the maximum at $+25$ mV. The voltage at which 50% of channels were activated was found to be -24 ± 14 mV ($n = 5$ neurons from three mice). Note different slopes with transition around -35 mV in both *I*–*V* curves and activation curve of I_D, consistent
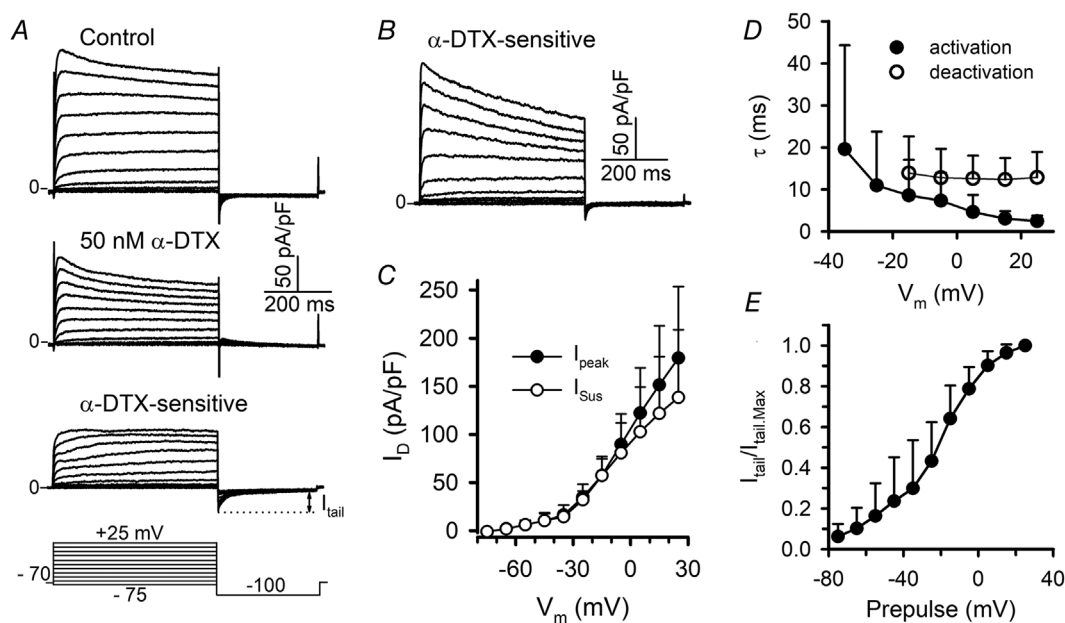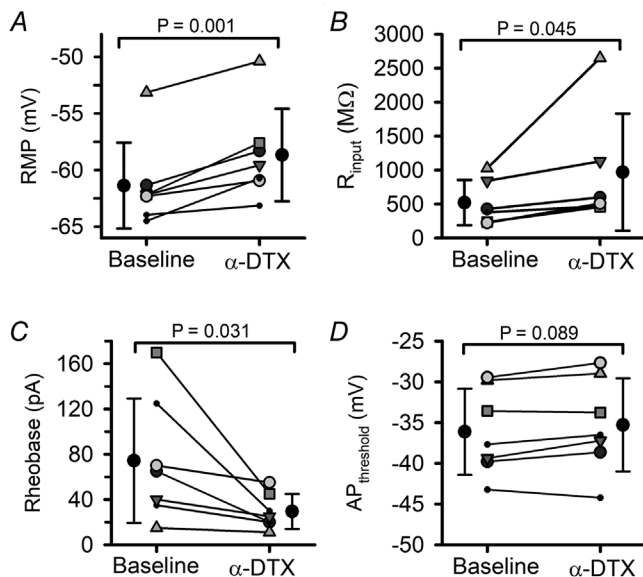

Figure 4. Voltage-dependent properties of I_D in mouse lung-specific nodose neurons
A, representative recordings of outward K$^+$ currents obtained from a WGA488-labelled neuron in the absence (Control) and presence of 50 nMα-DTX with the voltage-clamp protocol shown at the bottom. The α-DTX-sensitive current, defined as I_D, was obtained by digital subtraction of the currents recorded in α-DTX from those recorded before application of α-DTX. *B*, the family of α-DTX-sensitive currents obtained from another lung-specific nodose neuron showing slow inactivation. *C*, *I*–*V* curves of peak and sustained I_D, I_{peak} and I_{sus}, obtained from six neurons isolated from three mice. *D*, mean activation and deactivation time constants (τ) of I_D, obtained from six and five neurons, respectively (from three mice), plotted against the step voltages. *E*, mean activation curves obtained from five neurons of three mice. Pooled data in *C*–*E* are expressed as means $\pm$ SD.

with the two outward components observed in the voltage ramp-elicited I_D currents.

Effects of α-DTX on the excitability of nodose neurons innervating the mouse lungs

To evaluate the role of I_D channels in the regulation of bronchopulmonary vagal sensory neuron excitability, we examined the effects of α-DTX on the membrane properties and action potential firings in lung-specific nodose neurons. Bath application of 50 nMα-DTX significantly depolarized the resting potential ($P = 0.001$), increased the input resistance around the resting potential ($P = 0.045$), and significantly reduced the rheobase ($P = 0.031$) while having no effects on the voltage threshold ($P = 0.089$) for AP generation (Fig. 5A–D). AP firing in response to 600-ms depolarization induced by injecting 100–500 pA depolarizing currents was studied in six lung-specific nodose neurons (from three mice). At baseline, 2/6 neurons generated no more than one AP in response to injected currents of different intensities whereas the other four neurons fired multiple APs. Application of α-DTX significantly increased the number of AP discharge (Fig. 6A) and rendered the neurons with phasic AP firing generating more tonic firing of APs in response to suprathreshold depolarization (Fig. 6B). α-DTX significantly increased the number of APs evoked

Table 2. Effects of α-DTX on the peak and time course of AHP in bronchopulmonary nodose neurons ($n = 6$ neurons from three mice)

Current steps (pA)	Baseline	α-DTX	P
	Peak of AHP (mV)		
200	-71.1 ± 4.0	-70.1 ± 3.9	0.181
300	-68.9 ± 4.4	-66.8 ± 4.2	0.012
400	-66.0 ± 5.4	-64.3 ± 5.5	0.047
500	-64.3 ± 5.6	-62.0 ± 5.7	0.043
	Rate of decay (mV ms^{-1})		
200	2.68 ± 0.72	3.25 ± 0.69	0.008
300	3.60 ± 0.70	4.35 ± 0.96	0.011
400	4.27 ± 0.83	5.27 ± 0.98	0.003
500	5.14 ± 1.34	5.83 ± 0.14	0.005

Data are means $\pm$ SD. *P*-values determined by paired *t*-test.

by all five tested intensities of depolarizing currents (Fig. 6C, $P = 0.034$, 0.012, 0.024, 0.028 and 0.016 for 100 pA through 500 pA current injections), and modestly increased the peak frequency of AP firings, derived from the shortest interspike interval, in response to the depolarizing currents that elicited multiple APs (Fig. 6D, $P = 0.025$, 0.008 and 0.002 for 300 pA through 500 pA current injections).

Since the amplitude and the time course of after-hyperpolarization (AHP) directly impact the AP firing frequency, we analysed the effect of α-DTX on the peak of AHP and the rate of AHP decay during the AP firing in response to step currents. The peak of AHP was measured at the steady state during repetitive firing or for the first AP (depending on the AP firing patterns) before and after the application of α-DTX. The rate of AHP decay was determined by fitting the decay phase of AHP of the first AP to a linear function. The results are shown in Table 2. Inhibition of I_D caused a modest but significant decrease (i.e. less negative) in the peak of AHP ($P = 0.012$, 0.047 and 0.043 for action potentials elicited by current steps of 300, 400 and 500 pA, respectively), and increased the rate of AHP decay ($P = 0.008$, 0.011, 0.003 and 0.005 for APs evoked by current steps of 200 through 500 pA). These results indicate that I_D channels play an important role in promoting the adaptation of AP firings in lung-specific nodose neurons.


Figure 5. Effects of α-DTX on the membrane properties and excitability of bronchopulmonary nodose neurons
A–*D*, resting membrane potential (RMP), input resistance (R_{input}), rheobase and voltage threshold of AP firing (AP$_{threshold}$), respectively, at baseline and in the presence of 50 nMα-DTX. Each pair of interconnected symbols shows the results obtained in individual neurons. The filled circles and error bars represent the mean $\pm$ SD of group data. Statistical method: paired *t*-test.

Effects of α-DTX on the excitability of nodose afferent nerve terminals in mouse lungs

To evaluate whether I_D channels play a role in regulating the excitability of the nodose bronchopulmonary afferent nerve terminals, we examined the effects of α-DTX on the afferent nerve activation using *ex vivo*

vagally innervated trachea–lungs preparations excised from *Pirt-Cre;R26-GCaMP6s* transgenic mice and the two-photon microscopic Ca^{2+} imaging technique (Patil et al., 2019). Action potentials generated at the afferent terminals in the lungs propagate along vagus to the soma located in the vagal ganglia on their way to their central terminals in the brainstem. The AP opens the voltage-gated Ca^{2+} channels resulting in Ca^{2+} influx in the soma which then binds to the genetically encoded Ca^{2+}-sensing protein GCaMP6s leading to increased GCaMP6s fluorescence which can be captured by the two-photon microscope. Figure 7A shows the representative live two-photon microscopic images of a nodose ganglia sub-stack obtained at baseline and following applications of buffer, α-DTX, α,β-mATP and capsaicin via trachea to the lungs. The intensity of the green fluorescence is a function of the number of APs conducted to the soma from the nerve terminals in the lungs (Patil et al., 2020). Experiments were carried out on five lung–vagus nerve preparations. A total of 380 neurons from five nodose ganglia responded to α,β-mATP, and $60 \pm 17\%$ ($n = 5$ ganglia) of these neurons were capsaicin-sensitive, indicative of nodose C-fibres.

A total of 216 nerve fibres were found to be activated by applying 100 nM α-DTX to the lungs. One hundred and forty-two out of 216 α-DTX-sensitive neurons were also responsive to 10 μM α,β-mATP. This indicates that ~70% of the α-DTX-responsive nerve terminals were likely to be ATP-sensitive nodose nerves, with the rest being either jugular nerves or α,β-mATP-resistant nodose nerves (Nassenstein et al., 2010; Wang et al., 2017). We found that 50% of the capsaicin-sensitive nodose C-fibres were activated by α-DTX. Among the capsaicin-insensitive nodose nerves, 32% responded to α-DTX (these nerves likely comprise capsaicin-insensitive C-fibres and A-fibres) (Fig. 7B).

The relative amplitudes of increase in the fluorescence signal in response to α-DTX *vs.* to α,β-mATP and capsaicin applied to the lungs were analysed in 100 airway nodose neurons that responded to all three agents (recorded from five ganglia of five mice). Figure 7C shows the representative Ca^{2+} transients obtained from 10 neurons. The pooled data given in Fig. 7D show that the Ca^{2+} increase in response to α-DTX is significantly lower than that to α,β-mATP or capsaicin ($P < 0.001$ and $P = 0.009$, respectively), indicating that the number
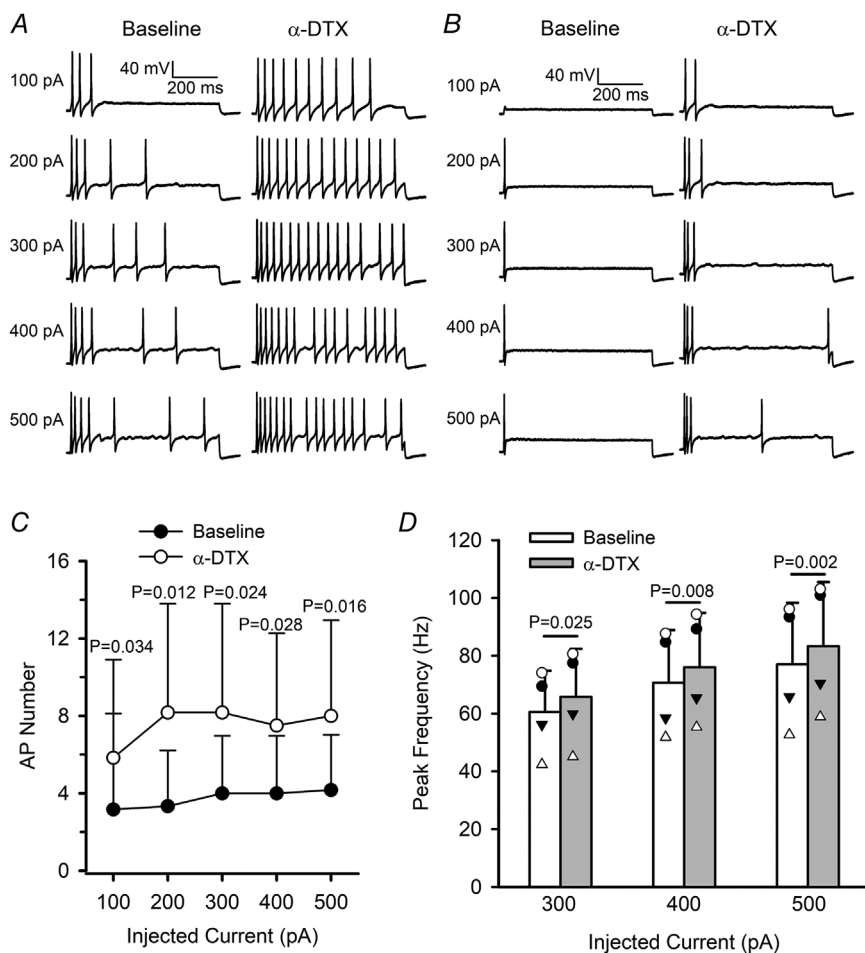
Figure 6. Effects of α-DTX on the AP firing properties of mouse bronchopulmonary nodose neurons
A and *B*, representative recordings of AP firing obtained from two different neurons in response to five levels of depolarizing current injection (as indicated on the left side of traces) at baseline and in the presence of 50 nM α-DTX. The RMP was −63.4 mV and −60.2 mV at baseline and with α-DTX, respectively, for the neuron in *A*, and −62.4 mV and −57.2 mV at baseline and with α-DTX, respectively, for the neuron in *B*. C, averaged AP numbers (mean ± SD, $n = 6$ neurons from three mice) obtained at baseline and in the presence of α-DTX are plotted against the amplitude of injected depolarizing currents. *P*-values were from paired *t*-test. D, bar graph showing the averaged peak frequency of AP firing, derived from the shortest interspike interval, in response to different amplitude of injected depolarizing currents at baseline and in the presence of 50 nM α-DTX ($n = 4$ neurons from two mice). Results obtained from individual neurons are given with different symbols on the bars. Each type of symbol depicts the data obtained from the same neuron. *P*-values were the results of paired *t*-test.

and/or the frequency of AP firings caused by inhibition of I_D channels was less than that evoked by the maximal α,β-mATP- or capsaicin-induced stimulation. The similar amplitudes of increase in the fluorescence signals induced by α,β-mATP and capsaicin ($P = 0.339$) observed in this group of neurons are consistent with our previous studies (Patil et al., 2019, 2020).

The imaging technique described above is ideally suited to provide information on the prevalence of afferent nerves responding to a given stimulus, but it is incapable of obtaining information on the conduction velocity of the responding nerves, or the precise AP numbers and peak frequency of AP discharges. For this type of granular detail, we employed extracellular electrophysiological recordings of single nerve fibre activities in the *ex vivo* trachea–lungs–vagus nerve preparation to quantify the effect of α-DTX. In these studies, we focused on nodose C-fibres (conduction velocity of 0.54 ± 0.04 m s^{-1}, $n = 19$ C-fibres from 19 mice). Tracheal perfusion of α-DTX (300 nм in 1 ml volume applied in ∼20 s) evoked AP discharge in 8 of 19 C-fibres (42%) terminating in the

mouse lungs. The response was variable ranging from 8 to 169 APs (mean 63 ± 64) and the peak frequency of AP discharge was 4.4 ± 3.9 Hz ($n = 8$ fibres from eight mice). One example is shown in Fig. 8. The same eight C-fibres responded to 10 μм α,β-mATP with significantly ($P = 0.041$) higher peak AP firing frequency averaging 11.5 ± 6.6 Hz.

Discussion

To the best of our knowledge, this is the first study investigating the function of D-type K$^+$ channels in the regulation of bronchopulmonary vagal afferent nerve excitability. Our main findings include (1) nearly all bronchopulmonary nodose afferent neurons express the α-DTX-sensitive K$_V$1.1, K$_V$1.2 or K$_V$ 1.6 α-subunits; (2) I_D channels contribute to setting the resting membrane potential, counterbalancing the subthreshold depolarization and promoting the accommodation of action potential discharge in nodose neurons innervating
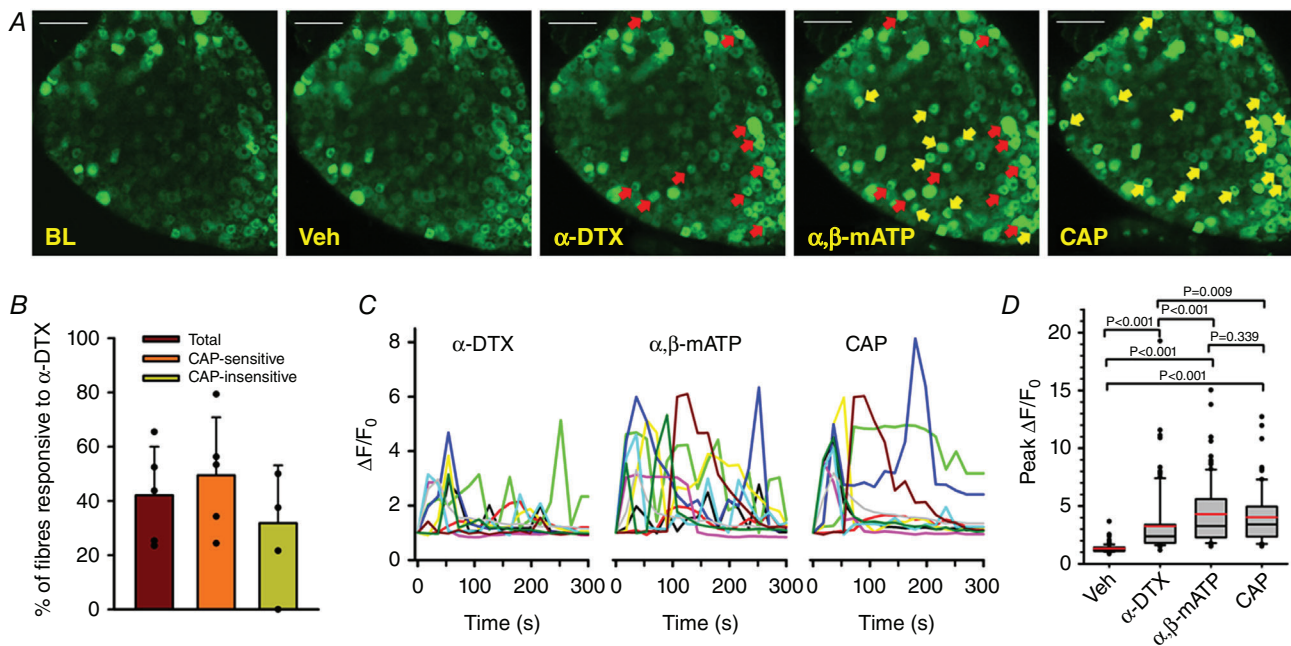
**Figure 7. Effects of α-DTX on the activity of mouse bronchopulmonary nodose afferent nerves**

A, representative live two-photon microscopic images (one *z*-sub-stack) obtained from a nodose ganglion of *Pirt-Cre;R26GCaMP6s* transgenic mouse at baseline and in response to vehicle (Veh), 100 nм α-DTX, 10 μмα,β-mATP and 1 μм capsaicin (CAP) applied to the lungs via trachea (3 ml volume in 1 min). Increased green fluorescence indicates the propagation of APs generated at the nerve terminals to the cell soma. White bars on the images represent 100 μm. Red arrowheads indicate neurons responsive to α-DTX (middle panel) or to both α-DTX and α,β-mATP (fourth panel from left). Yellow arrowheads indicate neurons responsive to α,β-mATP but not to α-DTX (fourth panel) and neurons responsive to capsaicin (rightmost panel). *B*, prevalence of response of nodose nerve terminals (α,β-mATP-responsive) in the lungs to α-DTX. $n = 5$ ganglia. *C*, representative Ca^{2+} transients caused by AP firing from 10 nerve fibres terminated to all three compounds as indicated. *D*, box and whisker plot of Ca^{2+} transient amplitude in response to vehicle, α-DTX, α,β-mATP and capsaicin obtained from 100 bronchopulmonary nodose neurons (from five ganglia of five mice) that responded to all three compounds. The red lines in the boxes indicate mean values. One way repeated measures analysis of variance with Holm–Šidák method for all pairwise multiple comparisons was performed for statistical analyses.

the mouse lungs; and (3) bronchopulmonary nodose C-fibre afferent nerve terminals express functional I_D channels, and inhibition of I_D is sufficient to evoke AP discharge in a substantial portion of these nerves.

I_D has been described in the peripheral sensory neurons from nodose (Glazebrook et al., 2002; McFarlane & Cooper, 1991; Stansfeld et al., 1986, 1987), dorsal root (Everill et al., 1998; Gold et al., 1996; Gonzalez et al., 2017), trigeminal (Madrid et al., 2009; Yoshida & Matsumoto, 2005) and petrosal ganglia (Kline et al., 2005). It was often referred to as the slowly inactivating A-type K^+ current (I_{As}) in earlier studies (Gold et al., 1996; McFarlane & Cooper, 1991; Stewart et al., 2003; Yoshimura & de Groat, 1999; Yoshimura et al., 1996). In some other studies, the low-threshold K^+ currents, which contain both I_A and I_D, have been broadly named I_A (Dang et al., 2004; Xu et al., 2006). It is now, however, well established that the I_A and I_D channels have different molecular bases, as well as distinct inactivation properties, pharmacological profiles and functional roles (Gutman et al., 2005; Harvey, 2001; McFarlane & Cooper, 1991; Ovsepian et al., 2016; Yoshimura et al., 1996; Zemel et al., 2018). The unique pharmacological properties of I_D have become the key for dissection of this current in the native neurons. Studies in the heterologous expression systems have revealed that α-DTX has a high affinity for $K_V1.1$, $K_V1.2$ and $K_V1.6$ channels (Harvey, 2001). It inhibits the cloned $K_V1.1$ expressed in oocytes with an IC_{50} of 1.1–12 nM, $K_V1.2$ IC_{50} of 0.4–4 nM, and $K_V1.6$ IC_{50} of 9–25 nM, while other K_V1 α-subunits as well as K_V3 and K_V4 channels are much less sensitive to this neurotoxin ($IC_{50} >100$–600 nM for $K_V1.3$, >200 nM for $K_V1.4$ and $K_V1.5$, >100 nM for K_V3s and >300 nM for $K_V4.1$) (Harvey, 2001). Studies in native neurons have reported that α-DTX at concentrations up to 500 nM and 1 μM did not inhibit I_A in nodose and dorsal root ganglia neurons,

respectively (Everill et al., 1998; Stansfeld et al., 1987). In rat hippocampus neurons, 300 nM α-DTX does not affect M-currents, Ca^{2+}-activated K^+ currents or I_q currents (Halliwell et al., 1986). Therefore, the 50 nM α-DTX we used in patch clamp studies can be considered selective for the I_D channels. It should be pointed out that we used higher concentrations of α-DTX (100 nM $\times$ 3 ml or 300 nM $\times$ 1 ml) to study the effects of inhibiting I_D channels on bronchopulmonary afferent nerve terminals in the *ex vivo* vagally innervated trachea–lung preparations. In this preparation a bolus of the toxin was applied via trachea to the lungs in an open superfused system. The concentration of α-DTX at the level of the nerve terminal biophase is some undefined concentration appreciably lower than the original infused concentration.

Our results showed that the activation threshold of I_D in the bronchopulmonary nodose neurons is slightly more negative than their resting potentials. Consistent with this property, α-DTX caused modest but significant membrane depolarization and increased the input resistance measured around the resting potential. These findings are not limited to the lung-specific nodose neurons. We have previously demonstrated that inhibition of I_D by 50 nM α-DTX or 60 μM 4-AP led to a similar degree of membrane depolarization and increase in the input resistance in randomly selected mouse nodose C-fibre and A-fibre neurons (Sun, 2021). Membrane depolarization as a result of I_D inhibition has also been observed in adult rat nodose neurons (Stansfeld et al., 1986), but not seen in neonatal rat nodose neurons where the voltage threshold for I_D activation was around -45 mV (Glazebrook et al., 2002). The $V_{1/2}$ for I_D activation found in mouse bronchopulmonary nodose neurons (-24 mV) in this study also appears to be more negative than the -17.6 and -2 mV found in the neonatal rat nodose neurons (Glazebrook et al., 2002; McFarlane & Cooper, 1991). Based on published studies, the effects of I_D channel inhibition on the resting potential appear to be cell type-dependent. It has been reported that α-DTX or $K_V1.1$-sensitive DTX-K does not cause membrane depolarization in sensory neurons isolated from adult rat trigeminal or dorsal root ganglia (DRG) (Chi & Nicol, 2007; Yoshida & Matsumoto, 2005). In the central nervous system, inhibition of I_D by α-DTX depolarized the octopus cells in the cochlear nucleus by $\sim$6 mV (Bal & Oertel, 2001; Cao & Oertel, 2017), but had no effect on the resting potentials in neocortical pyramidal neurons (Guan et al., 2007; Pathak et al., 2016). These observations may reflect different voltage thresholds for I_D activation in different types of neurons. Different major α-subunit compositions of the channels in different type of neurons may contribute to this discrepancy. The native neuronal α-DTX-sensitive K^+ channels are mainly heterotetramers composed of α-DTX-sensitive $K_V1.1$, $K_V1.2$, $K_V1.6$, and less frequently the α-DTX-insensitive
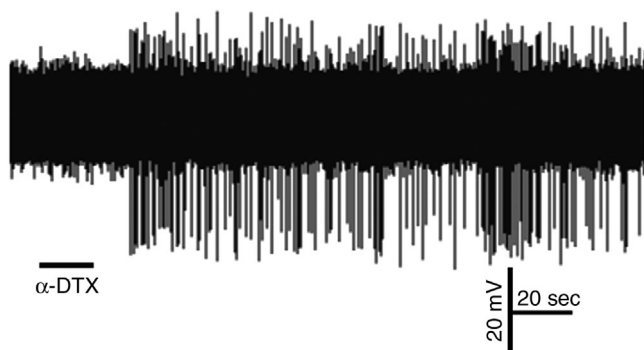
Figure 8. Example of lung nodose C-fibre response to α-DTX assessed with extracellular recording technique
The α-DTX applied as a bolus (300 nM, 1 ml within 20 s) to the lungs via trachea evoked AP firing in this fibre with a peak frequency of 8 Hz and a total of 169 APs. This fibre also responded to α,β-mATP and had a conduction velocity of 0.4 m s^{-1}.

$K_V 1.4$ or $K_V 1.3$ α-subunits (Coleman et al., 1999; Koch et al., 1997; Rasband et al., 2001; Scott et al., 1994; Shamotienko et al., 1997; Wang et al., 1999). Studies in the heterologous expression systems have revealed that the heterotetrameric I_D channels with different α-subunit compositions and/or different stoichiometry of contributing subunits exhibit different biophysical properties such as different inactivation kinetics and voltage threshold of activation (Hopkins et al., 1994; Ruppersberg et al., 1990; Sokolov et al., 2007). Specifically, $K_V 1.2/1.6$ channels activate at more negative voltages than $K_V 1.1/1.2$ channels (Sokolov et al., 2007). In rat DRG neurons, the $K_V 1.1$ and $K_V 1.2$ mRNA are highly abundant while $K_V 1.3$, $K_V 1.4$, $K_V 1.5$ and $K_V 1.6$ are detected at lower levels (Yang et al., 2004), consistent with the most abundant co-expression of $K_V 1.1$ and $K_V 1.2$ α-subunits identified by quantitative immunostaining (Rasband et al., 2001). The subunit composition of I_D channels in vagal sensory neurons has not been reported. Our single-neuron RT-PCR experiments showed that the $K_V 1.6$ transcript was most prevalently expressed in both randomly selected mouse nodose neurons and lung-specific nodose neurons. The same finding has been reported in adult rat nodose neurons (Glazebrook et al., 2002). Analysis of the RNAseq data made available by Mazzone et al. (2020) reveals that, in the mouse bronchopulmonary nodose neurons expressing the corresponding *Kcna* genes, *Kcna6*/$K_V 1.6$ is most abundantly expressed (3444 cpm), followed by *Kcna2*/$K_V 1.2$ (1845 cpm), then *Kcna4*/$K_V 1.4$ (335 cpm) and *Kcna1*/$K_V 1.1$ (324 cpm). Thus, the expression profile of I_D channel α-subunits in vagal sensory neurons appears to be different from that found in DRG neurons. It is tempting to speculate that the major I_D channel α-subunit composition in nodose neurons may be $K_V 1.2/K_V 1.6$ and that explains the more negative activation threshold.

The I_D channel activates rapidly and displays little inactivation at membrane potential ≤ -15 mV in mouse bronchopulmonary nodose neurons. The activation time constant was voltage-dependent and averaged 7.3 ± 2.5 ms at -5 mV and 2.6 ms at $+25$ mV. These values are similar to those obtained from neonatal rat nodose neurons (Glazebrook et al., 2002; McFarlane & Cooper, 1991). Low threshold, fast activation and lack of inactivation render the I_D channel an effective inhibitor of subthreshold depolarization, as evidenced by the significant reduction in rheobase without changes in the AP threshold after the channel was inhibited by α-DTX. The neuronal excitability is controlled by the concerted action of various excitatory and inhibitory ion channels available at resting and/or subthreshold potentials. The finding that inhibition of I_D channels led to AP discharge in 40−50% of afferent nerve fibres terminating in the mouse lungs suggests that the I_D channel may be the major inhibitory mechanism against

the excitatory currents at the subthreshold voltages in these neurons. Indeed, we found that I_D current accounted for $\geq 50\%$ of total K$^+$ current at voltages between -55 and -45 mV in the bronchopulmonary nodose neurons. Our results also show that inhibition of I_D increased the AP number and peak firing frequency in bronchopulmonary nodose neurons in response to sustained depolarizing current steps, accompanied by a modest decrease of the peak of AHP and increased rate of AHP decay. Since the peak of AHP is at voltages beyond or just at the activation threshold of I_D channels, the current flowing through the relatively slowly closing I_D channels upon repolarization from the peak of AP will play a role in influencing the peak and time course of AHP. Consistent with this inference, we found that the deactivation time constant of I_D channels in the bronchopulmonary nodose neurons was $12-14$ ms. This largely covers the duration between the peak of AP and the time AHP returns to -60 mV (7.6 ± 1.0 ms in response to the 200 pA sustained current step). Increased AP firing as a result of I_D inhibition appears to be a consistent observation in various types of neurons examined for this effect (Chi & Nicol, 2007; Glazebrook et al., 2002; Guan et al., 2007; Pathak et al., 2016; Wang et al., 2016; Yoshida & Matsumoto, 2005).

The vagal C-fibres in mouse lungs comprise both nodose and jugular C-fibres, with nodose C-fibres predominating (Nassenstein et al., 2010). The fact that nodose and jugular C-fibres possess distinct nerve phenotypes can complicate mechanistic studies. Unlike jugular C-fibres, we know of stimuli that only activate the mouse nodose fibres. For example, in the mouse, nodose C-fibres can be readily distinguished from jugular C-fibres by their responsiveness to the PAR1 agonist and to ATP (Kwong et al., 2008; Wang et al., 2017), allowing for an analysis of nodose C-fibres uncontaminated by jugular C-fibre input. Therefore, in this study we focused our attention specifically on bronchopulmonary nodose C-fibres. Nevertheless, the α-DTX-sensitive Kv1 α-subunits are expressed by both C-fibre subtypes (Mazzone et al., 2020), so the information gained from our analysis of I_D channels in the nodose C-fibres likely has relevance to vagal C-fibres in general.

Despite their importance, there have been only a few studies looking into the changes or functions of voltage-gated potassium channels in airway vagal sensory neurons (Gu et al., 2009; McAlexander & Undem, 2000; Sun et al., 2019; Zhang et al., 2013). Most of these investigations did not explicitly identify the nature of specific K_V channel type(s) under study or their molecular counterparts (Gu et al., 2009; McAlexander & Undem, 2000; Zhang et al., 2013). The present study demonstrates that in the mouse, I_D channels, mainly composed of the α-DTX-sensitive $K_V 1.1$, $K_V 1.2$ and $K_V 1.6$ α-subunits, act as a critical brake on the activation of bronchopulmonary

vagal afferents, including nodose C-fibres. These findings are consistent with the hypothesis that a decrease in I_D may contribute to enhanced C-fibre activity in airway diseases that are associated with excessive coughing, dyspnoea, and reflex bronchospasm and secretions. In this regard it is noteworthy that down-regulation of I_D channel α-subunits and/or reduced I_D currents in DRG sensory neurons has been reported in chronic nerve injuries (Gonzalez et al., 2017; Kim et al., 2002; Park et al., 2003; Yang et al., 2004; Zhao et al., 2013), diabetic neuropathy (Wang et al., 2016) and inflammatory diseases of various visceral organs (Dang et al., 2004; Stewart et al., 2003; Xu et al., 2006; Yoshimura & de Groat, 1999), and shown to be associated with pain and hyperexcitability. Our finding that I_D is a major 'brake' on excitability of airway nociceptive C-fibre neurons is also consistent with the supposition that selective openers of the I_D channels may provide substantive benefit for those suffering from chronic cough, chronic obstructive pulmonary disease and hyper-reactive airway diseases, as we have previously argued for with respect to certain KCNQ channel openers (Sun et al., 2019). An advantage of targeting these maladies is that the potassium channel openers can be delivered topically to the airway nerves via inhalation thereby reducing unwanted effects of systemic potassium channel manipulation.

References

Bal, R., & Oertel, D. (2001). Potassium currents in octopus cells of the mammalian cochlear nucleus. *Journal of Neurophysiology*, **86**(5), 2299–2311.

Brew, H. M., Gittelman, J. X., Silverstein, R. S., Hanks, T. D., Demas, V. P, Robinson, L. C., Robbins, C. A., McKee-Johnson, J., Chiu, S. Y., Messing, A., & Tempel, B. L. (2007). Seizures and reduced life span in mice lacking the potassium channel subunit Kv1.2, but hypoexcitability and enlarged Kv1 currents in auditory neurons. *Journal of Neurophysiology*, **98**(3), 1501–1525.

Cao, X. J., & Oertel, D. (2017). Genetic perturbations suggest a role of the resting potential in regulating the expression of the ion channels of the KCNA and HCN families in octopus cells of the ventral cochlear nucleus. *Hearing Research*, **345**, 57–68.

Catacuzzeno, L., Fioretti, B., Pietrobon, D., & Franciolini, F. (2008). The differential expression of low-threshold K$^+$ currents generates distinct firing patterns in different subtypes of adult mouse trigeminal ganglion neurones. *The Journal of Physiology*, **586**(21), 5101–5118.

Chi, X. X., & Nicol, G. D. (2007). Manipulation of the potassium channel Kv1.1 and its effect on neuronal excitability in rat sensory neurons. *Journal of Neurophysiology*, **98**(5), 2683–2692.

Coleman, S. K., Newcombe, J., Pryke, J., & Dolly, J. O. (1999). Subunit composition of Kv1 channels in human CNS. *Journal of Neurochemistry*, **73**(2), 849–858.

Dang, K., Bielefeldt, K., & Gebhart, G. F. (2004). Gastric ulcers reduce A-type potassium currents in rat gastric sensory ganglion neurons. *American Journal of Physiology. Gastrointestinal and Liver Physiology*, **286**(4), G573–G579.

Everill, B., Rizzo, M. A., & Kocsis, J. D. (1998). Morphologically identified cutaneous afferent DRG neurons express three different potassium currents in varying proportions. *Journal of Neurophysiology*, **79**(4), 1814–1824.

Glazebrook, P. A., Ramirez, A. N., Schild, J. H., Shieh, C. C., Doan, T., Wible, B. A., & Kunze, D. L. (2002). Potassium channels Kv1.1, Kv1.2 and Kv1.6 influence excitability of rat visceral sensory neurons. *The Journal of Physiology*, **541**(2), 467–482.

Gold, M. S., Shuster, M. J., & Levine, J. D. (1996). Characterization of six voltage-gated K$^+$ currents in adult rat sensory neurons. *Journal of Neurophysiology*, **75**(6), 2629–2646.

Gonzalez, A., Ugarte, G., Restrepo, C., Herrera, G., Pina, R., Gomez-Sanchez, J. A., Pertusa, M., Orio, P, & Madrid, R. (2017). Role of the excitability brake potassium current IKD in cold allodynia induced by chronic peripheral nerve injury. *The Journal of Neuroscience*, **37**(12), 3109–3126.

Grundy, D. (2015). Principles and standards for reporting animal experiments in The Journal of Physiology and Experimental Physiology. *The Journal of Physiology*, **593**(12), 2547–2549.

Gu, Q., Lim, M. E., Gleich, G. J., & Lee, L. Y. (2009). Mechanisms of eosinophil major basic protein-induced hyperexcitability of vagal pulmonary chemosensitive neurons. *American Journal of Physiology. Lung Cellular and Molecular Physiology*, **296**(3), L453–L461.

Guan, D., Lee, J. C., Higgs, M. H., Spain, W. J., & Foehring, R. C. (2007). Functional roles of Kv1 channels in neocortical pyramidal neurons. *Journal of Neurophysiology*, **97**(3), 1931–1940.

Gutman, G. A., Chandy, K. G., Grissmer, S., Lazdunski, M., McKinnon, D., Pardo, L. A., Robertson, G. A., Rudy, B., Sanguinetti, M. C., Stuhmer, W., & Wang, X. (2005). International Union of Pharmacology. LIII. Nomenclature and molecular relationships of voltage-gated potassium channels. *Pharmacological Reviews*, **57**(4), 473–508.

Halliwell, J. V., Othman, I. B., Pelchen-Matthews, A., & Dolly, J. O. (1986). Central action of dendrotoxin: Selective reduction of a transient K conductance in hippocampus and binding to localized acceptors. *Proceedings of the National Academy of Sciences, USA*, **83**(2), 493–497.

Hao, J., Padilla, F., Dandonneau, M., Lavebratt, C., Lesage, F., Noel, J., & Delmas, P. (2013). Kv1.1 channels act as mechanical brake in the senses of touch and pain. *Neuron*, **77**(5), 899–914.

Harvey, A. L. (2001). Twenty years of dendrotoxins. *Toxicon*, **39**(1), 15–26.

Hopkins, W. F., Allen, M. L., Houamed, K. M., & Tempel, B. L. (1994). Properties of voltage-gated K$^+$ currents expressed in Xenopus oocytes by mKv1.1, mKv1.2 and their heteromultimers as revealed by mutagenesis of the dendrotoxin-binding site in mKv1.1. *Pflugers Archiv: European Journal of Physiology*, **428**(3–4), 382–390.

Kim, D. S., Choi, J. O., Rim, H. D., & Cho, H. J. (2002). Downregulation of voltage-gated potassium channel alpha gene expression in dorsal root ganglia following chronic constriction injury of the rat sciatic nerve. *Brain Research Molecular Brain Research*, **105**(1–2), 146–152.

Kleopa, K. A., Elman, L. B., Lang, B., Vincent, A., & Scherer, S. S. (2006). Neuromyotonia and limbic encephalitis sera target mature Shaker-type K$^+$ channels: subunit specificity correlates with clinical manifestations. *Brain*, **129**(6), 1570–1584.

Kline, D. D., Buniel, M. C., Glazebrook, P., Peng, Y. J., Ramirez-Navarro, A., Prabhakar, N. R., & Kunze, D. L. (2005). Kv1.1 deletion augments the afferent hypoxic chemosensory pathway and respiration. *The Journal of Neuroscience*, **25**(13), 3389–3399.

Koch, R. O., Wanner, S. G., Koschak, A., Hanner, M., Schwarzer, C., Kaczorowski, G. J., Slaughter, R. S., Garcia, M. L., & Knaus, H. G. (1997). Complex subunit assembly of neuronal voltage-gated K$^+$ channels. Basis for high-affinity toxin interactions and pharmacology. *The Journal of Biological Chemistry*, **272**(44), 27577–27581.

Kollarik, M., & Undem, B. J. (2004). Activation of bronchopulmonary vagal afferent nerves with bradykinin, acid and vanilloid receptor agonists in wild-type and TRPV1-/- mice. *The Journal of Physiology*, **555**(1), 115–123.

Kullmann, D. M., & Hanna, M. G. (2002). Neurological disorders caused by inherited ion-channel mutations. *The Lancet Neurology*, **1**(3), 157–166.

Kwong, K., Kollarik, M., Nassenstein, C., Ru, F., & Undem, B. J. (2008). P2×2 receptors differentiate placodal vs. neural crest C-fiber phenotypes innervating guinea pig lungs and esophagus. *American Journal of Physiology. Lung Cellular and Molecular Physiology*, **295**(5), L858–L865.

Lee, L. Y., & Yu, J. (2014). Sensory nerves in lung and airways. *Comprehensive Physiology*, **4**, 287–324.

Madrid, R., de laPena, E., Donovan-Rodriguez, T., Belmonte, C., & Viana, F. (2009). Variable threshold of trigeminal cold-thermosensitive neurons is determined by a balance between TRPM8 and Kv1 potassium channels. *The Journal of Neuroscience*, **29**(10), 3120–3131.

Mazzone, S. B., Tian, L., Moe, A. A. K., Trewella, M. W., Ritchie, M. E., & McGovern, A. E. (2020). Transcriptional profiling of individual airway projecting vagal sensory neurons. *Molecular Neurobiology*, **57**(2), 949–963.

Mazzone, S. B., & Undem, B. J. (2016). Vagal afferent innervation of the airways in health and disease. *Physiological Reviews*, **96**(3), 975–1024.

McAlexander, M. A., & Undem, B. J. (2000). Potassium channel blockade induces action potential generation in guinea-pig airway vagal afferent neurones. *Journal of the Autonomic Nervous System*, **78**(2–3), 158–164.

McFarlane, S., & Cooper, E. (1991). Kinetics and voltage dependence of A-type currents on neonatal rat sensory neurons. *Journal of Neurophysiology*, **66**(4), 1380–1391.

Nassenstein, C., Taylor-Clark, T. E., Myers, A. C., Ru, F., Nandigama, R., Bettner, W., & Undem, B. J. (2010). Phenotypic distinctions between neural crest and placodal derived vagal C-fibres in mouse lungs. *The Journal of Physiology*, **588**(23), 4769–4783.

Ovsepian, S. V., LeBerre, M., Steuber, V., O'Leary, V. B., Leibold, C., & Oliver Dolly, J. (2016). Distinctive role of KV1.1 subunit in the biology and functions of low threshold K$^+$ channels with implications for neurological disease. *Pharmacology & Therapeutics*, **159**, 93–101.

Park, S. Y., Choi, J. Y., Kim, R. U., Lee, Y. S., Cho, H. J., & Kim, D. S. (2003). Downregulation of voltage-gated potassium channel alpha gene expression by axotomy and neurotrophins in rat dorsal root ganglia. *Molecules and Cells*, **16**, 256–259.

Pathak, D., Guan, D., & Foehring, R. C. (2016). Roles of specific Kv channel types in repolarization of the action potential in genetically identified subclasses of pyramidal neurons in mouse neocortex. *Journal of Neurophysiology*, **115**(5), 2317–2329.

Patil, M. J., Meeker, S., Bautista, D., Dong, X., & Undem, B. J. (2019). Sphingosine-1-phosphate activates mouse vagal airway afferent C-fibres via S1PR3 receptors. *The Journal of Physiology*, **597**(7), 2007–2019.

Patil, M. J., Ru, F., Sun, H., Wang, J., Kolbeck, R. R., Dong, X., Kollarik, M., Canning, B. J., & Undem, B. J. (2020). Acute activation of bronchopulmonary vagal nociceptors by type I interferons. *The Journal of Physiology*, **598**(23), 5541–5554.

Rasband, M. N., Park, E. W., Vanderah, T. W., Lai, J., Porreca, F., & Trimmer, J. S. (2001). Distinct potassium channels on pain-sensing neurons. *Proceedings of the National Academy of Sciences, USA*, **98**(23), 13373–13378.

Robbins, C. A., & Tempel, B. L. (2012). Kv1.1 and Kv1.2: Similar channels, different seizure models. *Epilepsia*, **53**(Suppl 1), 134–141.

Ruppersberg, J. P., Schroter, K. H., Sakmann, B., Stocker, M., Sewing, S., & Pongs, O. (1990). Heteromultimeric channels formed by rat brain potassium-channel proteins. *Nature*, **345**(6275), 535–537.

Scott, V. E., Muniz, Z. M., Sewing, S., Lichtinghagen, R., Parcej, D. N., Pongs, O., & Dolly, J. O. (1994). Antibodies specific for distinct Kv subunits unveil a heterooligomeric basis for subtypes of alpha-dendrotoxin-sensitive K$^+$ channels in bovine brain. *Biochemistry*, **33**(7), 1617–1623.

Shamotienko, O. G., Parcej, D. N., & Dolly, J. O. (1997). Subunit combinations defined for K$^+$ channel Kv1 subtypes in synaptic membranes from bovine brain. *Biochemistry*, **36**(27), 8195–8201.

Shen, W., Hernandez-Lopez, S., Tkatch, T., Held, J. E., & Surmeier, D. J. (2004). Kv1.2-containing K$^+$ channels regulate subthreshold excitability of striatal medium spiny neurons. *Journal of Neurophysiology*, **91**(3), 1337–1349.

Smart, S. L., Lopantsev, V., Zhang, C. L., Robbins, C. A., Wang, H., Chiu, S. Y., Schwartzkroin, P. A., Messing, A., & Tempel, B. L. (1998). Deletion of the K(V)1.1 potassium channel causes epilepsy in mice. *Neuron*, **20**(4), 809–819.

Sokolov, M. V., Shamotienko, O., Dhochartaigh, S. N., Sack, J. T., & Dolly, J. O. (2007). Concatemers of brain Kv1 channel alpha subunits that give similar K$^+$ currents yield pharmacologically distinguishable heteromers. *Neuropharmacology*, **53**(2), 272–282.

Stansfeld, C. E., Marsh, S. J., Halliwell, J. V., & Brown, D. A. (1986). 4-Aminopyridine and dendrotoxin induce repetitive firing in rat visceral sensory neurones by blocking a slowly inactivating outward current. *Neuroscience Letters*, **64**(3), 299–304.

Stansfeld, C. E., Marsh, S. J., Parcej, D. N., Dolly, J. O., & Brown, D. A. (1987). Mast cell degranulating peptide and dendrotoxin selectively inhibit a fast-activating potassium current and bind to common neuronal proteins. *Neuroscience*, **23**(3), 893–902.

Stewart, T., Beyak, M. J., & Vanner, S. (2003). Ileitis modulates potassium and sodium currents in guinea pig dorsal root ganglia sensory neurons. *The Journal of Physiology*, **552**(3), 797–807.

Storm, J. F. (1988). Temporal integration by a slowly inactivating K^+ current in hippocampal neurons. *Nature*, **336**(6197), 379–381.

Sun, H. (2021). Different sensitivity of action potential generation to the rate of depolarization in vagal afferent A-fiber versus C-fiber neurons. *Journal of Neurophysiology*, **125**(5), 2000–2012.

Sun, H., Lin, A. H., Ru, F., Patil, M. J., Meeker, S., Lee, L. Y., & Undem, B. J. (2019). KCNQ/M-channels regulate mouse vagal bronchopulmonary C-fiber excitability and cough sensitivity. *JCI Insight*, **4**(5), e124467.

Wang, F. C., Parcej, D. N., & Dolly, J. O. (1999). alpha subunit compositions of Kv1.1-containing K^+ channel subtypes fractionated from rat brain using dendrotoxins. *European Journal of Biochemistry*, **263**(1), 230–237.

Wang, J., Kollarik, M., Ru, F., Sun, H., McNeil, B., Dong, X., Stephens, G., Korolevich, S., Brohawn, P., Kolbeck, R., & Undem, B. (2017). Distinct and common expression of receptors for inflammatory mediators in vagal nodose versus jugular capsaicin-sensitive/TRPV1-positive neurons detected by low input RNA sequencing. *PLoS One*, **12**(10), e0185985.

Wang, X. C., Wang, S., Zhang, M., Gao, F., Yin, C., Li, H., Zhang, Y., Hu, S. J., & Duan, J. H. (2016). Alpha-Dendrotoxin-sensitive Kv1 channels contribute to conduction failure of polymodal nociceptive C-fibers from rat coccygeal nerve. *Journal of neurophysiology*, **115**(2), 947–957.

Xu, G. Y., Winston, J. H., Shenoy, M., Yin, H., & Pasricha, P. J. (2006). Enhanced excitability and suppression of A-type K^+ current of pancreas-specific afferent neurons in a rat model of chronic pancreatitis. *American Journal of Physiology. Gastrointestinal and Liver Physiology*, **291**(3), G424–G431.

Yang, E. K., Takimoto, K., Hayashi, Y., deGroat, W. C., & Yoshimura, N. (2004). Altered expression of potassium channel subunit mRNA and alpha-dendrotoxin sensitivity of potassium currents in rat dorsal root ganglion neurons after axotomy. *Neuroscience*, **123**(4), 867–874.

Yoshida, S., & Matsumoto, S. (2005). Effects of alpha-dendrotoxin on K^+ currents and action potentials in tetrodotoxin-resistant adult rat trigeminal ganglion neurons. *The Journal of Pharmacology and Experimental Therapeutics*, **314**(1), 437–445.

Yoshimura, N., & deGroat, W. C. (1999). Increased excitability of afferent neurons innervating rat urinary bladder after chronic bladder inflammation. *The Journal of Neuroscience*, **19**(11), 4644–4653.

Yoshimura, N., White, G., Weight, F. F., & deGroat, W. C. (1996). Different types of Na^+ and A-type K^+ currents in dorsal root ganglion neurones innervating the rat urinary bladder. *The Journal of Physiology*, **494**(1), 1–16.

Zemel, B. M., Ritter, D. M., Covarrubias, M., & Muqeem, T. (2018). A-type KV channels in dorsal root ganglion neurons: Diversity, function, and dysfunction. *Frontiers in Molecular Neuroscience*, **11**, 253.

Zhang, Z., Zhuang, J., Zhang, C., & Xu, F. (2013). Isoflurane depolarizes bronchopulmonary C neurons by inhibiting transient A-type and delayed rectifier potassium channels. *Respiratory Physiology & Neurobiology*, **186**, 164–172.

Zhao, X., Tang, Z., Zhang, H., Atianjoh, F. E., Zhao, J. Y., Liang, L., Wang, W., Guan, X., Kao, S. C., Tiwari, V., Gao, Y. J., Hoffman, P. N., Cui, H., Li, M., Dong, X., & Tao, Y. X. (2013). A long noncoding RNA contributes to neuropathic pain by silencing Kcna2 in primary afferent neurons. *Nature Neuroscience*, **16**(8), 1024–1031.

Additional information

Data availability statement

All data supporting the results in the paper are in the paper itself.

Competing interests

None.

Author contributions

Conception or design of the work: H.S., B.J.U. Acquisition, analysis or interpretation of data for the work: H.S., M.J.P., F.R., S.M., B.J.U. Drafting the work or revising it critically for important intellectual content: H.S., M.J.P., F.R., S.M., B.J.U. All authors have read and approved the final version of this manuscript and agree to be accountable for all aspects of the work in ensuring that questions related to the accuracy or integrity of any part of the work are appropriately investigated and resolved. All persons designated as authors qualify for authorship, and all those who qualify for authorship are listed.

Funding

Acknowledgements

Author's present address

M. J. Patil: Department of Molecular Pharmacology and Physiology, Morsani College of Medicine, University of South Florida, Tampa, FL, USA.

Supporting information

Additional supporting information can be found online in the Supporting Information section at the end of the HTML view of the article. Supporting information files available:

Peer Review History
Statistical Summary Document